

## Ion Migration Study on $\text{YAlO}_3$ -perovskite through Atomistic Simulations

---

Rubén O. Miranda-Rosales, J. Francisco Gómez-García\*

Departamento de Física y Química Teórica, Facultad de Química, UNAM. Circuito Exterior S/N, Ciudad Universitaria, C. P. 04510, Ciudad de México, Mexico.

\*Corresponding author: J. Francisco Gómez-García, email: [jfrancisco@comunidad.unam.mx](mailto:jfrancisco@comunidad.unam.mx)

Received April 13<sup>th</sup>, 2023; Accepted September 9<sup>th</sup>, 2023.

DOI: <http://dx.doi.org/10.29356/jmcs.v68i3.2047>

**Abstract.** In this work, we presented an atomistic simulation study on  $\text{YAlO}_3$  perovskite. We simulated the reported crystal structure through the energy minimization process from coulombic and Buckingham potentials with the General Utility Lattice Program (GULP). We determined the formation energy for all point pair defects presented in the system. We found that the anionic Frenkel together with Schottky pair defects are the main defects in the  $\text{YAlO}_3$  perovskite.

Additionally, we performed several energy profile migrations for each ion, and we determined that oxygen migration was the favored migration via the vacancy-vacancy path with 98.70 kJ/mol. In the end, we performed a series of calculations about doping energy, and we calculated that  $\text{Ca}^{2+}$  is the best aliovalent ion for doping  $\text{YAlO}_3$  compound, which involves the minimum doping energy while the aliovalent doping increases the oxygen vacancy defects. We suggested that these atomistic simulations could be used as a tool in the design or optimization of new materials for developing solid electrolytes.

**Keywords:**  $\text{YAlO}_3$  perovskite; atomistic simulations; point defect energy; ion migration.

**Resumen.** En este trabajo presentamos un estudio hecho por medio de simulaciones atomísticas para el compuesto  $\text{YAlO}_3$  con estructura perovskita. La estructura se simuló por medio de la minimización energética de los potenciales de Coulomb y de Buckingham. Se determinó la energía de formación para todos los pares de defectos puntuales que puede presentar el sistema y encontramos que los defectos tipo Frenkel aniónico y los Schottky son los principales en el compuesto de estudio. También determinamos los perfiles energéticos de migración para los iones en el sistema y encontramos que la migración de menor energía corresponde a la de oxígeno vía vacancia-vacancia con una energía de 98.70 kJ/mol. Hacia el final del artículo, presentamos los cálculos referentes a la energía de dopaje y encontramos que el mejor ion para dopar al compuesto  $\text{YAlO}_3$  es el ion  $\text{Ca}^{2+}$ ; esto debido a la menor energía de dopaje involucrada y el hecho de que el dopaje aliovalente incrementa las vacancias de oxígeno en el sistema. Sugerimos que este tipo de estudios pueden ser una herramienta muy versátil en el desarrollo y optimización de nuevos electrolitos sólidos.

**Palabras clave:** Perovskita  $\text{YAlO}_3$ ; simulaciones atomísticas; energía de defectos puntuales; migración de iones.

---

## Introduction

Solid Electrolytes (SE) are materials involved in many technological devices that are directly or indirectly related to renewable energy. Electrolyzers for water splitting [1], [2], electrochemical membranes for gas separation [3], and solid oxide fuel cells (SOFCs) for electricity generation [4] among others, are devices

where the electrolyte plays an important role due to the charge-mass transport. Developing better electrolyte materials will enhance the performance of the electrochemical devices and consequently, will consolidate an energy society with low-carbon fuels, whether hydrogen as an energetic vector is considered [5].

High-Temperature Solid Electrolytes (HTSE) display better performance in ionic transport than room-temperature ones. Additionally, when HTSE are used in electrochemical devices, these show fast catalytic response at electrodes which allows to use of materials based on oxides instead of Pt or Pd electrodes [6]. These characteristics get the attention of the research community for developing new HTSE for electrochemical devices and atomistic simulations could be a useful tool for exploring in silico which materials are candidates to bring out good electrical properties. Thus, in this work, we performed atomistic simulations in  $\text{YAlO}_3$  with perovskite structure since this crystal structure has the main characteristic for exhibiting ionic conductivity as close packed anion arranged together with ions in its high oxidation state which minimizes the electronic conductivity [7]. Besides this, perovskite-type structures could present proton conductivity, which is another form of ionic conductivity [8-10]. Also, we presented a doping study with aliovalent ions; as ionic conductivity depends on the charge carrier concentration, doping systems had the higher concentration [11] due to the extrinsic point defects are much bigger than intrinsic defects.

$\text{YAlO}_3$  exhibits a perovskite-like structure with octahedra tilting. The unit cell is orthorhombic with lattices parameters  $a = 5.33 \text{ \AA}$ ,  $b = 7.375 \text{ \AA}$  and  $c = 5.18 \text{ \AA}$ . This structure presents two crystal positions for oxygen ion, one at  $4c$  (0.475, 1/4, 0.586) and the other at  $8d$  (0.293, 0.044, 0.203) Wyckoff positions, while the cations present only one crystal position;  $4c$  (0.0526, 1/4, 0.4896) for  $\text{Y}^{3+}$  and  $4b$  (0, 0, 0) for  $\text{Al}^{3+}$ . The space group for this crystal structure was reported as  $Pnma$  (No. 62) [12].

Atomistic simulations had been employed to study ion diffusion pathways in several systems showing results very close to experimental values [13–16], thus we used this methodology in this work. Atomistic simulations were carried out using GULP code (version 5.2) [17], [18]. This code uses static modeling techniques based on the classical Born model for ionic solids, allowing the description in mathematical terms of the system energy as a function of particle coordinates. In this model, the integral charge of the ions corresponds to its oxidation state, and the energy interactions ( $V_{ij}$ ) between ions are calculated in terms of long-range coulombic forces and short-range pair potentials with the standard Buckingham potential. This potential simulates the electron cloud overlap (Pauli repulsion) and dispersion interactions (van der Waals) [13]. All these terms are included in equation 1, where  $\kappa$  is the Coulomb constant;  $q_i$  and  $q_j$  are the integral charges of the ions  $i$  and  $j$  respectively;  $r_{ij}$  is the inter-ionic distance and  $A_{ij}$ ,  $\rho_{ij}$ , and  $C_{ij}$  are empirical parameters assigned to each ion-ion interaction, except for the cation-cation interactions which were treated as purely coulombic.

$$V_{ij}(r_{ij}) = \frac{1}{2} \kappa \frac{q_i q_j}{r_{ij}} + A_{ij} \exp\left(\frac{-r_{ij}}{\rho_{ij}}\right) - \frac{C_{ij}}{r_{ij}^6} \quad (1)$$

## Results and discussion

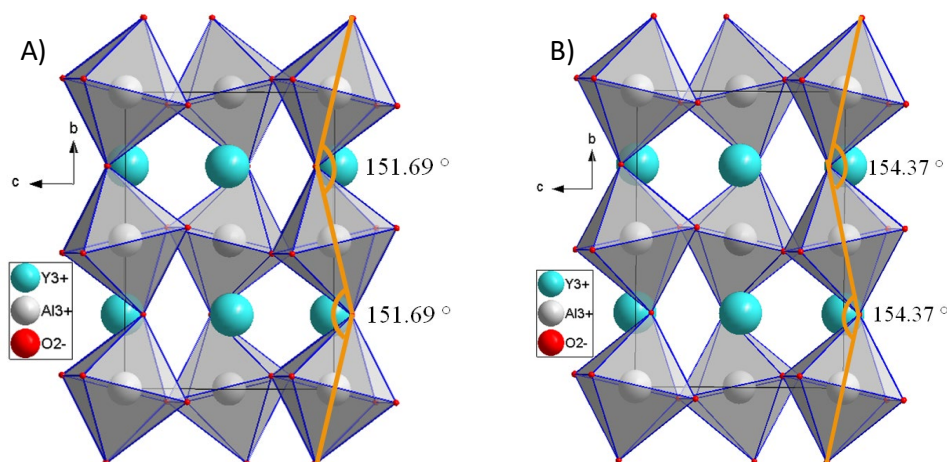
$\text{YAlO}_3$  perovskite crystal structure was calculated using Buckingham pair potentials previously reported for Y-O, O-O [19], and Al-O [20]. These potentials are listed in Table 1 together with core-shell parameters. Crystal structure results are showed in Table 2 where it can be seen that the calculated lattice parameters agreed with those previously reported by Diehl [12]. Calculated atomic coordinates (data not showed) also agreed with experimental ones as can be observed in Fig. 1, where not only coordination polyhedra were the same but the tilting angle was satisfactorily calculated after fitting the  $\rho$  Buckingham parameter for cation-anion interactions.

**Table 1.** Parameters used for  $\text{YAlO}_3$  crystal modeling with GULP, the potentials for Y-O, O-O pairs were taken from [19], and for Al-O pair from [20].

Ionic pair	$A$ [kJ/mol]	$\rho$ [Å]	$C$ [kJ/mol Å <sup>6</sup> ]	Ion	$Y^+$ [e]	$k$ [kJ/mol Å <sup>2</sup> ]
Y-O	126395.79	0.350865	0.00	$\text{Y}^{3+}$	0.0000	9648437.16
Al-O	232481.90	0.275805	0.00	$\text{Al}^{3+}$	0.0430	38978.15
O-O	2196421.15	0.1490	4148.87	$\text{O}^{2-}$	0.2389	4052.38

**Table 2.** Structural parameters comparison between reported and simulated structures.

Parameter	Reported	Simulated
$a$ [Å]	5.330	5.274
$b$ [Å]	7.375	7.406
$c$ [Å]	5.180	5.223
$V$ [Å <sup>3</sup> ]	203.619	204.031
$E_{\text{lattice}}$ [kJ/mol]	--	-14373.3

**Fig. 1.** (A) Reported and (B) calculated crystal structure for  $\text{YAlO}_3$  perovskite.

Since the calculated lattice was close to the experimental one, we performed point defect calculations to obtain the formation energy for associated point defects (Schottky and Frenkel defects). Point defects were calculated using the Mott-Littleton approximation [21] which splits the crystal into three spherical regions to optimize the calculations; the inner region, called Region 1, has the defect at the center, and the ions are strongly affected by the point defect. The ion positions in Region 1 must be calculated for each ion. In the next region, called Region 2a, the ions are slightly affected by the point defect and their positions can be calculated through a potential. In the outer region, called Region 2b, the ions are not affected by the point defect and do not contribute to the defect energy calculation. In this work we use a 14 Å radius for Region 1 and a 30 Å radius for Region 2a, this configuration allowed us to calculate the point defect energy considering the effect of 2300 ions around the point defect; usually, the Mott-Littleton approximation considers at least 300 ions for this kind

of calculations [22]. The calculated energy relative to points defects is listed in Table 3; the interstitial positions used in these calculations were (0.5,0.5,0) for  $Y^{3+}$ , (0.5395, 0.25, 0.25) for  $Al^{3+}$ , and (0.8616, 0.75, 0.875) for  $O^{2-}$ . In this table is possible to see that oxygen vacancy energy for the two crystallographic oxygen ions is very close between them because of the similar crystallo-chemical environment.

**Table 3.** Calculated point defects energy in  $YAlO_3$  perovskite.

Species	Energy [kJ/mol]	
	Vacancies	Interstitial
Y	4436.02	-2192.35
Al	5928.85	-4088.59
O <sub>1</sub>	2151.65	-1213.50
O <sub>2</sub>	2147.71	

We use standard Kröger-Vink defect notation to describe associated defects such as Schottky or Frenkel defects. Symbols as  $V_O^-$  or  $Y_{Al}^x$  are used to describe a single point defect; the main symbol indicates the specie at point defect (usually  $V$  is used for indicating a vacancy), subscript indicates the position in the lattice represented by the atom or ion occupying that site (interstitial positions are represented by  $i$ ), and superscript indicates the charge of the point defect, dots (·) for positive charge, dashes (‘) for negative, and (x) for neutral defects [23].

From point defect and lattice energy, it was possible to determine the formation energy for the intrinsic defects on the  $YAlO_3$  structure according to its corresponding formation reactions listed below in Kröger-Vink notation.



In these equations *null* indicates a perfect crystal without point defects so the formation energy for each intrinsic defect was calculated taking into account the *null* state as a reference value (0 kJ/mol) and, in the case of Schottky defect, lattice energy was considered in the equation due to mass conservation. A couple of examples of those calculations are presented below.

$$E_{Schottky} = \frac{1}{5} \left( E_{V_{Al}^m} + E_{V_Y^m} + E_{V_{O_1}^{2-}} + 2E_{V_{O_2}^{2-}} + E_{YAlO_3} \right) \quad \text{Schottky formation (6)}$$

$$E_{Frenkel,Al} = \frac{1}{2} \left( E_{V_{Al}^m} + E_{Al_i^{3+}} \right) \quad \text{Aluminum Frenkel formation (7)}$$

The energy defect formation is normalized to the total number of point defects formed in each reaction. The calculated values are listed in Table 4, where it can be seen that Schottky and anionic Frenkel defects are the most favoured and in consequence, the cationic and oxygen vacancies together with oxygen interstitial are the main defects present in the system.

**Table 4.** Associative defects energy in  $\text{YAlO}_3$  perovskite.

Associative defect	Energy/defect [kJ/mol]
Schottky	487.72
Frenkel Y	1121.83
Frenkel Al	920.13
Frenkel $\text{O}_1$	469.08
Frenkel $\text{O}_2$	467.11

Ionic migration calculations were performed firstly, in a linear path formed by two nearest vacancies, determining the energy for an interstitial defect placed along the linear path as can be seen in Fig. 2. Those defects generate a profile where the maximum energy is related to the migration energy in the diffusion process, and then, to the activation energy in the electrical conductivity process [24]. Ionic migration (from vacancy to vacancy) calculations were carried out by  $\text{Al}^{3+}$ ,  $\text{Y}^{3+}$ , and  $\text{O}^{2-}$  species and minimum energy migration results were 413.15 kJ/mol, 926.45 kJ/mol, and 105.16 kJ/mol, respectively. As the oxygen ion migration had a minimal value, the rest of the calculations were focused only on this ion.

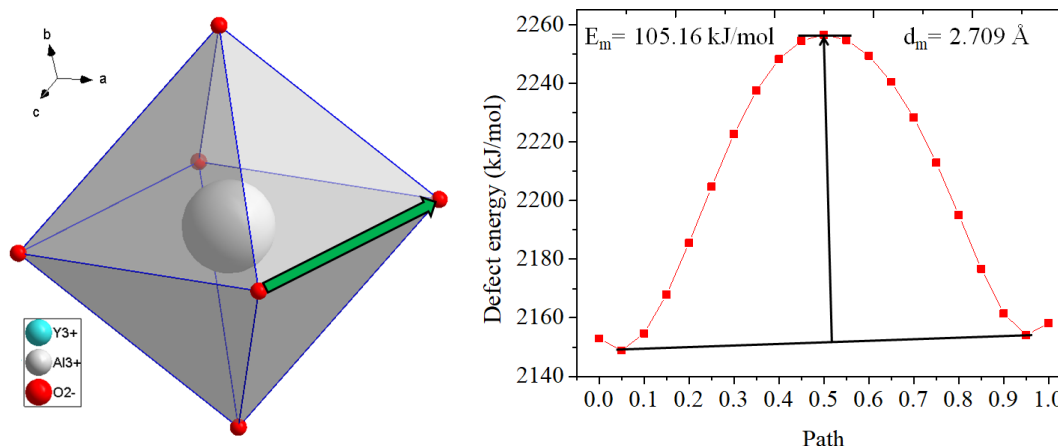


**Fig. 2.** Path and energetic profile migration due to oxygen ion migration in  $\text{YAlO}_3$  compound.

The linear path does not always result in the best path due to the steric effect between ions. In perovskite structure has been reported the presence of a “saddle point” [25] which consists of a space where the steric effects due to  $\text{Al}^{3+}$  and  $\text{Y}^{3+}$  on oxygen ion are minimal, the size of the saddle point is defined by the critical radius ( $r_{\text{crit}}$ ) showed in Fig. 3. In the ideal case, the linear path must contain the saddle point, but due to the Al—O bond length decreases as the path becomes close to the saddle point, it is necessary to evaluate alternative paths in which steric effects are minimal. In this scenario, we calculated the interstitial energy at the saddle point near and far from the  $\text{Al}^{3+}$  (the octahedra center) this is outlined in Fig. 3.

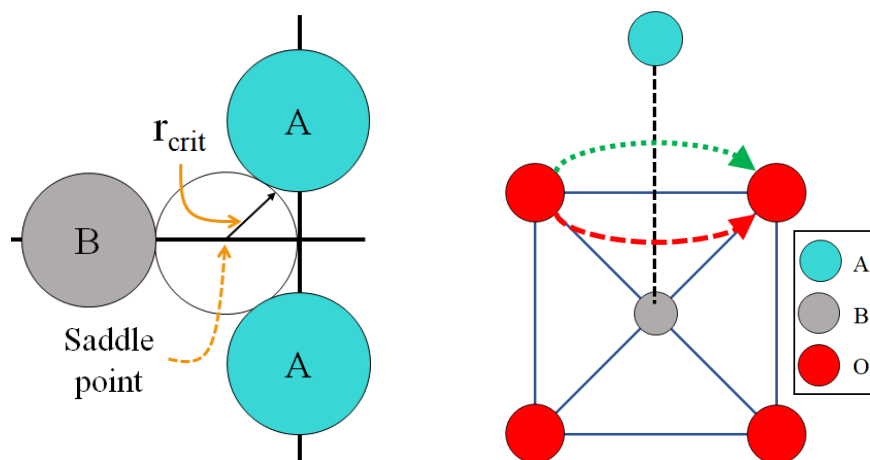


**Fig. 3.** Variation of the migration path for oxygen ions due to the saddle point in perovskite structures.

In the ideal perovskite structure, the saddle point, A sites, and B site positions are in the same plane, but, since  $\text{YAIO}_3$  is a distorted perovskite, saddle point, A, and B sites are not in the same plane and in consequence there are two ways to evaluate an alternative oxygen migration around  $\text{Al}^{3+}$ , one with the saddle point aligned with  $\text{Al}^{3+}$  site (red points in Fig. 4) and a second one aligning the saddle point with  $\text{Y}^{3+}$  positions (black points in Fig. 4). As can be observed in Fig. 4, no matter which of the paths are used, both had a minimum at the same point which is outer from the  $\text{AlO}_6$  octahedra. Additionally, as those calculations were made in the middle of the path, it can be assumed that each point corresponds to the maximum energy for a nonlinear path. A plot of migration energy as a function of the distance of the saddle point was made (Fig. 4), where the minimum migration energy of 98.70 kJ/mol was obtained for migration outside of the octahedra.

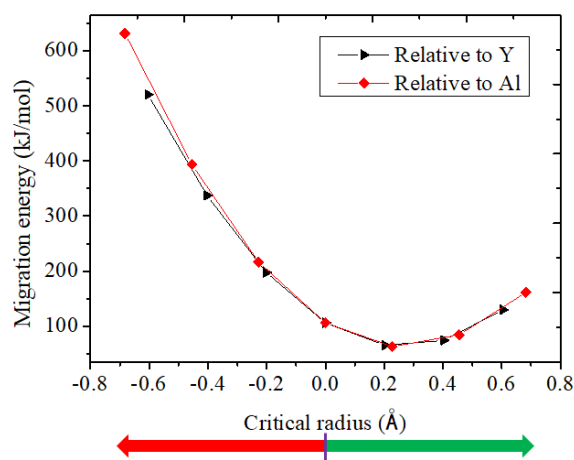


**Fig. 4.** Oxygen migration around  $\text{Al}^{3+}$  taking into account the saddle point effect.

Considering the Frenkel disorder, oxygen migration could take place through vacancy and interstitial defect, moreover, the atomistic simulations showed this migration is not favoured by its high migration energy (about 765.03 kJ/mol), but it was calculated that interstitial-interstitial migration had a 98.70 kJ/mol migration energy which is similar to the vacancy-vacancy oxygen migration showed in Fig. 4. According to simulations, oxygen is the main charge carrier in the system because it presents the minimal migration energy; the path

migration could be via vacancy-vacancy in a nonlinear path through the saddle point or via interstitial-interstitial in a linear path; moreover, the presence of oxygen interstitial it would unlikely due to the lack of chemically favoured sites for oxygen ions because the perovskite structure can be seen as a close packed arrangement of oxygen and yttrium ions and the aluminum cations took the octahedra holes [26]. Thus, oxygen migration via vacancy vacancy would be the main way for ionic transport.

High ionic conductivity in SE usually is related to the high concentration of charge carriers, but this is very low when charge carriers come from intrinsic point defects. Doped compounds are usually the solution to enhance the amount of charge carriers, because they keep the same crystal structure, and then, the same migration energy, but the number of point defects can be adjusted according to chemical reaction. Often, doping occurs via aliovalent doping (when a substitution occurs with an ion with a different charge but similar size) and doping the A-site in the perovskite structure yields oxygen vacancies according to the reaction (8) where an oxide with general formula MO is considered.



According to Shannon radii, aliovalent cations for  $Y^{3+}$  (1.019 Å) are  $Ca^{2+}$ ,  $Mg^{2+}$ , and  $Zn^{2+}$  whose ionic radii are 1.12 Å, 0.89 Å, and 0.9 Å respectively [27], thus these cations could be used for doping  $YAlO_3$  perovskite. Atomistic simulations made possible the determination of doping energy according to equation (9) which had been obtained from the reaction (8).

$$E_{doping} = E_{M'_Y} + \frac{1}{2} E_{V_O^{**}} - E_{lattice}^{MO} \quad (9)$$

The crystal structure parameters for CaO, MgO, and ZnO were previously reported [28] and lattice energy was calculated from GULP to determine the energy doping for each aliovalent ion, the results are listed in Table 5 where it can be seen that doping  $YAlO_3$  with  $Ca^{2+}$  implicates the lower energy thus the  $Y_{1-x}Ca_xAlO_{3-x/2}$  system would be the thermodynamically favored system among those formed with the aliovalent ions studied in this work. It would be important to mention that the  $Ca^{2+}$  crystal radius is closer to that for  $Y^{3+}$ , which can be related to the lower doping energy for the  $Y_{1-x}Ca_xAlO_{3-x/2}$  system.

**Table 5.** Doping energy for different aliovalent ions.

Doping ion	Ionic radius (Å)	Doping energy (kJ/mol)
$Ca^{2+}$	1.12	4507.12
$Mg^{2+}$	0.89	4570.60
$Zn^{2+}$	0.90	4570.51

The method employed in this work could be used as a tool for designing new materials where ionic transport is an important feature. Atomistic simulations require nonexpensive computing infrastructure and results can easily correlated with crystal structure and chemical properties and these calculations can optimize the selection criteria process in the research of new materials for ionic transport.

## Conclusions

We successfully simulated the  $YAlO_3$  crystal structure from electrostatic long-range interactions together with short-range Buckingham potentials. The lattice energy calculated was -14373.3 kJ/mol.

Additionally, formation energy for Schottky and Frenkel pair defects was calculated, and we determined that Schottky defects together with anionic Frenkel defects are the main point defects present in the  $\text{YAlO}_3$  structure due to its low formation energy: 487.72 kJ/mol for Schottky disorder and 467.11 kJ/mol for Frenkel disorder. Considering the point defects present in the compound, we performed migration calculation and we found that the lower migrations energy corresponded to oxygen ion migration via vacancy-vacancy and interstitial-interstitial site with 98.70 kJ/mol in both cases. In the end, we performed atomistic simulations to calculate the doping energy involved in the  $\text{Y}_{1-x}\text{M}_x\text{AlO}_{3-x/2}$  system with  $\text{M} = \text{Ca}^{2+}$ ,  $\text{Mg}^{2+}$ , and  $\text{Zn}^{2+}$ ; we found  $\text{Y}_{1-x}\text{Ca}_x\text{AlO}_{3-x/2}$  system had the minimum doping energy which implied that was the thermodynamically favored system. All these calculations allowed to us select one system in which structural and chemical properties could bring out interesting electrical properties.

## Acknowledgements

The author thanks to the DGAPA-UNAM project number IA208421 for financial support.

## References

1. Xiang, C.; Papadantonakis, K. M.; Lewis, N. S. *Mater. Horizons*. **2016**, 3, 169-173. DOI: <https://doi.org/10.1039/C6MH00016A>.
2. Tang, J.; Xu, X.; Tang, T.; Zhong, Y.; Shao, Z. *Small Methods*. **2022**, 6, 2201099. DOI: <https://doi.org/10.1002/smt.202201099>.
3. Vermaak, L.; Neomagus, H. W. J. P.; Bessarabov, D. G. *Membranes (Basel)*. **2021**, 11, 127. DOI: <https://doi.org/10.3390/membranes11020127>.
4. Dokiya, M. *Solid State Ionics*. **2002**, 152-153, 383-392. DOI: [https://doi.org/10.1016/S01672738\(02\)00345](https://doi.org/10.1016/S01672738(02)00345).
5. Oliveira, A. M.; Beswick, R. R.; Yan, Y. *Curr. Opin. Chem. Eng.* **2021**, 33, 100701. DOI: <https://doi.org/10.1016/j.coche.2021.100701>.
6. Shi, H.; Su, C.; Ran, R.; Cao, J.; Shao, Z. *Prog. Nat. Sci. Mater. Int.* **2020**, 30 (6), 764-774. DOI: <https://doi.org/10.1016/j.pnsc.2020.09.003>.
7. Haile, S. M. *Acta Mater.* **2003**, 51, 5981-6000. DOI: <https://doi.org/10.1016/j.actamat.2003.08.004>.
8. Bonanos, N. *Solid State Ionics*. **2001**, 145, 265-274. DOI: [https://doi.org/10.1016/S01672738\(01\)00951-1](https://doi.org/10.1016/S01672738(01)00951-1).
9. Fop, S. *J. Mater. Chem. A*. **2021**, 9, 18836-18856. DOI: <https://doi.org/10.1039/D1TA03499E>.
10. Meng, Y.; Gao, J.; Zhao, Z.; Amoroso, J.; Tong, J.; Brinkman, K. S. *J. Mater. Sci.* **2019**, 54, 9291-9312. DOI: <https://doi.org/10.1007/s10853-019-03559-9>.
11. Kilner, J. *Solid State Ionics*. **2000**, 129, 13-23. DOI: [https://doi.org/10.1016/S0167-2738\(99\)00313-6](https://doi.org/10.1016/S0167-2738(99)00313-6).
12. Diehl, R.; Brandt, G. *Mater. Res. Bull.* **1975**, 10, 85-90. [https://doi.org/10.1016/0025-5408\(75\)90125-7](https://doi.org/10.1016/0025-5408(75)90125-7).
13. Walker, A. M.; Wright, K.; Slater, B. *Phys. Chem. Miner.* **2003**, 30, 536-545. DOI: <https://doi.org/10.1007/s00269-003-0358-7>.
14. De Souza, R. A.; Maier, J. *Phys. Chem. Chem. Phys.* **2003**, 5, 740-748. DOI: <https://doi.org/10.1039/b209062g>.
15. Chroneos, A.; Yildiz, B.; Tarancón, A.; Parfitt, D.; Kilner, J. A. *Energy Environ. Sci.* **2011**, 4, 2774. DOI: <https://doi.org/10.1039/c0ee00717j>.
16. Wang, X.; Santos Carballal, D.; de Leeuw, N. H. *Phys. Chem. Chem. Phys.* **2023**, 25, 6797-6807. DOI: <https://doi.org/10.1039/D2CP04126J>.
17. Gale, J. D. *Philos. Mag. Part B*. **1996**, 73, 3-19. DOI: <https://doi.org/10.1080/13642819608239107>.

18. Gale, J. D.; Rohl, A. L. *Mol. Simul.* **2003**, 29, 291-341. DOI: <https://doi.org/10.1080/0892702031000104887>.
19. Ruiz Trejo, E. *Solid State Ionics.* **1999**, 123, 121-129. DOI: [https://doi.org/10.1016/S0167-2738\(99\)00092-2](https://doi.org/10.1016/S0167-2738(99)00092-2).
20. Bush, T. S.; Gale, J. D.; Catlow, C. R. A.; Battle, P. D. *J. Mater. Chem.* **1994**, 831. DOI: <https://doi.org/10.1039/jm9940400831>.
21. Mott, N. F.; Littleton, M. J. *Trans. Faraday Soc.* **1938**, 34, 485. DOI: <https://doi.org/10.1039/tf9383400485>.
22. Saiful Islam, M. *J. Mater. Chem.* **2000**, 10, 1027-1038. DOI: <https://doi.org/10.1039/a908425h>.
23. Yet Ming, C. in: *Physical Ceramics: Principles for Ceramics Science and Engineering*; John Wiley & Sons, Inc., **1997**.
24. Gómez Garcia, J. F. in: *Estudio Del Transporte Eléctrico En El Bronce de Niobio: CeNb3O9*, Universidad Nacional Autónoma de México, **2010**.
25. Kilner, J.; Brook, R. *Solid State Ionics* 1982, 6 (3), 237-252. DOI: <https://doi.org/10.1016/0167252>.
26. Woodward, P. M. *Acta Crystallogr. Sect. B Struct. Sci.* **1997**, 53 (1), 32-43. DOI: <https://doi.org/10.1107/S0108768196010713>.
27. Shannon, R. D. *Acta Crystallogr. Sect. A.* **1976**, 32, 751-767. DOI: <https://doi.org/10.1107/S0567739476001551>.
28. Wyckoff, R. in: *Crystal Structures*; Interscience Publishers: New York, New York, **1963**.